Journal of Power Sources 189 (2009) 1284–1291

Contents lists available at ScienceDirect

Journal of Power Sources

journal homepage: www.elsevier.com/locate/jpowsour

Influence of the mesoporous structure on capacitance of the RuO_2 electrode

Kentaro Kuratani, Tetsu Kiyobayashi*, Nobuhiro Kuriyama

Research Institute for Ubiquitous Energy Devices, National Institute of Advanced Industrial Science and Technology (AIST), 1-8-31, Midorigaoka, Ikeda, Osaka 563-8577, Japan

ARTICLE INFO

Article history:
Received 18 July 2008
Received in revised form 12 December 2008
Accepted 22 December 2008
Available online 30 December 2008

Keywords:
Ruthenium oxide
Capacitor
Mesoporous structure
Cyclic voltammetry
Electrochemical impedance spectroscopy

ABSTRACT

The difference in capacitive performance between high and low surface area RuO_2 electrodes, synthesized with and without a mesoporous silica template, respectively, was investigated in aqueous solutions of sulfuric acid and sulfates by cyclic voltammetry (CV) and electrochemical impedance spectroscopy (EIS). RuO_2 synthesized with the template was crystalline and the formation of the mesoporous structure with a 6.5 nm diameter was confirmed using a transmission electron microscope and the nitrogen adsorption and desorption isotherm. From the CV at the scan rate of 1 mV s^{-1}, the specific capacitance of the high surface area electrode in H_2SO_4(aq) was determined to be 200 F g^{-1}. The high surface area RuO_2 has a three times higher BET specific surface area (140 m^2 g^{-1}) than the low surface area sample (39 m^2 g^{-1}). Introducing the mesoporous structure was proved effective for increasing the capacitance per mass of the RuO_2, though not all the surface functions as a capacitor. Both the CV and EIS suggest that by increasing the charging rate or frequency, the mesoporous structure of the electrode leads to a lower capacitance decrease (higher capacitance retention) than the low surface area electrode. The EIS also indicates that the response time of the capacitor is hardly influenced by the presence of the mesoporous structure.

1. Introduction

With increasing interest in high power devices, electrochemical capacitors have attracted much attention due to their higher power density and longer cycle life than batteries, and higher energy density than conventional dielectric capacitors [1–4]. In electrochemical capacitors, carbon powder [5–7], conducting polymers [8–10] or conducting metal oxides [11–14] are widely used as the active materials. Carbon powder with a high specific surface area greater than 1000 m^2 g^{-1} is conventionally used in electric double layer capacitors (EDLCs), whose capacitance arises from the charge separation at the electrode–electrolyte interface [15]. On the other hand, conducting polymers and metal oxides store charges through the faradic redox reactions called pseudocapacitance [15]. Among these materials, conducting polymers and metal oxides with high surface areas are considered promising energy storage materials because the pseudocapacitors surpass the EDLCs in terms of the per interfacial area capacitance [16]. For instance, amorphous RuO_2 electrodes achieved the capacitance of ca. 700 F g^{-1} or 700 μF cm^{-2} in an aqueous H_2SO_4 electrolyte [11] which is more than 20 times greater than the double layer carbon electrodes typically having a capacitance of 30 μF cm^{-2}.

Introducing porous structures is a strategy used to develop conducting polymers and/or conducting metal oxides with a high specific surface area. Various conducting materials with porous structures have been synthesized and used as the electrodes of electrochemical capacitors [17–24]. For example, Liu and Anderson synthesized porous nickel oxide film by a sol–gel method. The obtained film showed the specific capacitance of 50–65 F g^{-1} [25]. Fusalba et al. achieved the specific capacitance of about 70 F g^{-1} by producing a porous structure in poly(cyclopenta[2,1-b;3,4-b′]dithiophen-4-one) [26]. Although these studies are intended to attain a high specific capacitance with porous structures, how the porous structure determines the capacitive behavior is still not fully understood [27–29].

The objective of the present study is to prepare electrodes with and without mesopores in order to quantitatively examine how the presence of the mesoporous structure influences their capacitive behavior. We used RuO_2, a pseudocapacitive metal oxide, as the active electrode material, because pseudocapacitors have such a high capacitance per surface area that the difference in the electrochemical properties produced by the mesopores must be more discernible than for the EDLCs as mentioned above. The electrochemical properties of the RuO_2 electrodes were investigated in aqueous solutions of sulfuric acid and sulfates by cyclic

* Corresponding author. Tel.: +81 72 7519651; fax: +81 72 7519629.
E-mail address: kiyobayashi-t@aist.go.jp (T. Kiyobayashi).

0378-7753/$ – see front matter © 2009 Elsevier B.V. All rights reserved.
doi:10.1016/j.jpowsour.2008.12.087

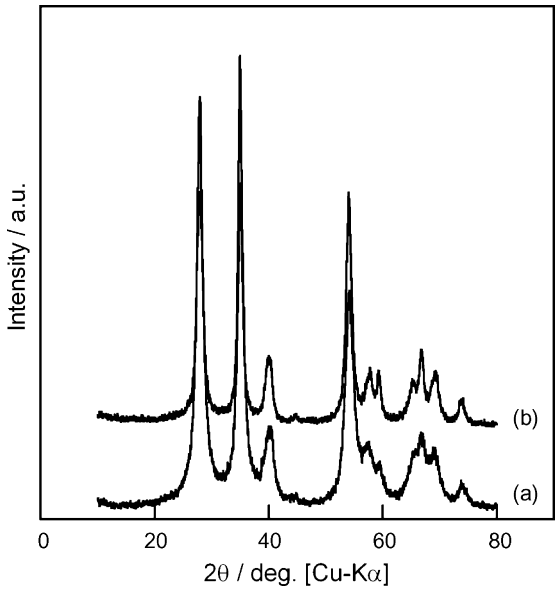

Fig. 1. X-ray diffraction patterns of the samples synthesized (a) with and (b) without KIT-6.

voltammetry (CV) and electrochemical impedance spectroscopy (EIS).

2. Experimental

2.1. Preparation and characterization of RuO_2 samples

High surface area RuO_2 was synthesized using KIT-6, a mesoporous silica, as a hard template. The KIT-6 was prepared according to the procedure reported by Ryoo and co-workers [30,31]. For the typical synthesis of the high surface area RuO_2, 0.48 g of ruthenium (III) chloride hydrate ($RuCl_3{\cdot}mH_2O$; Kishida Chemical) was dissolved in 30 cm^3 of ethanol (Kishida Chemical) followed by the addition of 1 g of KIT-6. The mixture was stirred at 343 K to evaporate the ethanol. The remaining powder was then slowly heated to 573 K and calcined at that temperature for 5 h in air. After the calcination, the powder was dispersed in 50 cm^3 of a 2.0 mol dm^{-3} sodium hydroxide solution and stirred overnight to remove the silica template. The obtained black powder was centrifuged, repeatedly washed with distilled water, and dried at 353 K overnight. The low surface area RuO_2 was prepared using the above procedure without KIT-6. For comparison, we also prepared the amorphous RuO_2 using a previously reported procedure [11] for the high capacitance: 0.3 mol dm^{-3} NaOH(aq) was dropwise added in 0.1 mol dm^{-3} $RuCl_3$(aq). The solution was stirred overnight and the precipitate was filtered off. The obtained powder was dried overnight at room temperature in air, then heated to 423 K for 17 h in air.

The crystal structure of the sample was characterized using a Rigaku RINT-2200 powder X-ray diffractometer (XRD) with Cu Kα radiation (λ = 0.154056 nm). The microstructure of the sample was examined using a Hitachi S-5000 scanning electron microscope (SEM) operated at 20 kV and a Jeol JEM-3000F transmission electron microscope (TEM) operated at 300 kV. The nitrogen adsorption and desorption isotherms were measured at 77 K with a Micromeritics ASAP 2010 system.

Table 1
BET surface areas of RuO_2 materials prepared (a) with and (b) without KIT-6. Total surface area is divided into two components: surface area attributable to the pore size of 1–2 nm "microstructure" and that of larger than 2 nm "mesostructure". Value in parentheses is the contribution from the pore diameter of 6.5 ± 1.5 nm to the "mesostructure" surface area.

	Total	1–2 nm	<2 nm
Sample (a) (HSA)	140	40	100 (30)
Sample (b) (LSA)	39	9	30

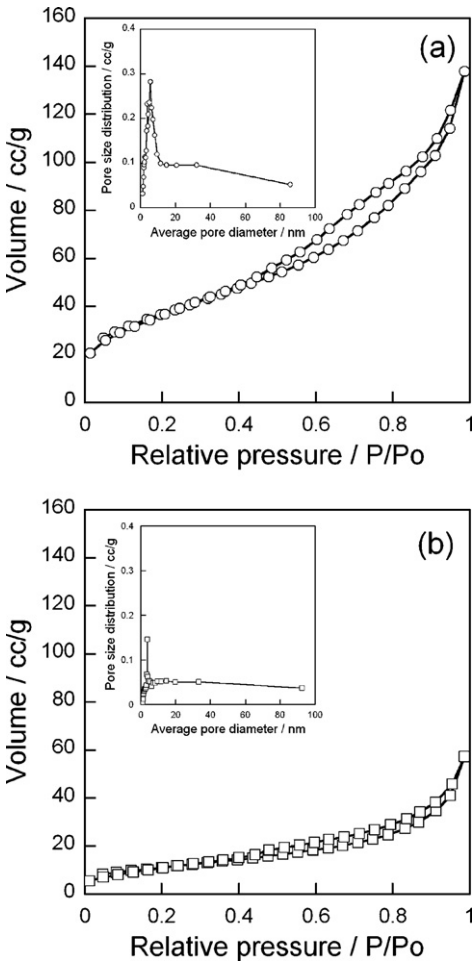

Fig. 2. Nitrogen adsorption and desorption isotherms of the samples prepared (a) with and (b) without KIT-6. The inset indicates the pore size distribution calculated from the desorption isotherm.

2.2. Electrochemical measurement of RuO_2 electrodes

The electrode for the electrochemical measurement was made by mixing 80 wt.% RuO_2, 10 wt.% acetylene black as a conductive additive, and 10 wt.% polyvinylidenedifluoride-*N*-methyl-2-pyrrolidone (PVdF-NMP) as a binder. The slurry was then spread onto Ti foil, followed by drying at 383 K under vacuum. The CV and EIS were conducted using an ALS CHI 608B electrochemical analyzer with a three-electrode setup. A Pt plate and the saturated calomel electrode (SCE) were used as the counter and reference electrodes, respectively. An aqueous solution of 0.5 mol dm^{-3} M_2SO_4, where M = H, Li, Na or K, was used as the electrolyte. CV was performed between –0.1 and 0.9 V vs. SCE at the scan rates of 1, 10, 20, 50 and 100 mV s^{-1}. EIS was carried out at 0.1 V vs. SCE, at which the RuO_2 electrodes show an ideal capacitive behavior with the amplitude of 10 mV in the frequency range from 10 kHz to 10 mHz. In order to confirm the reproducibility of the experiment, we prepared three specimens from different batches for each measurement.

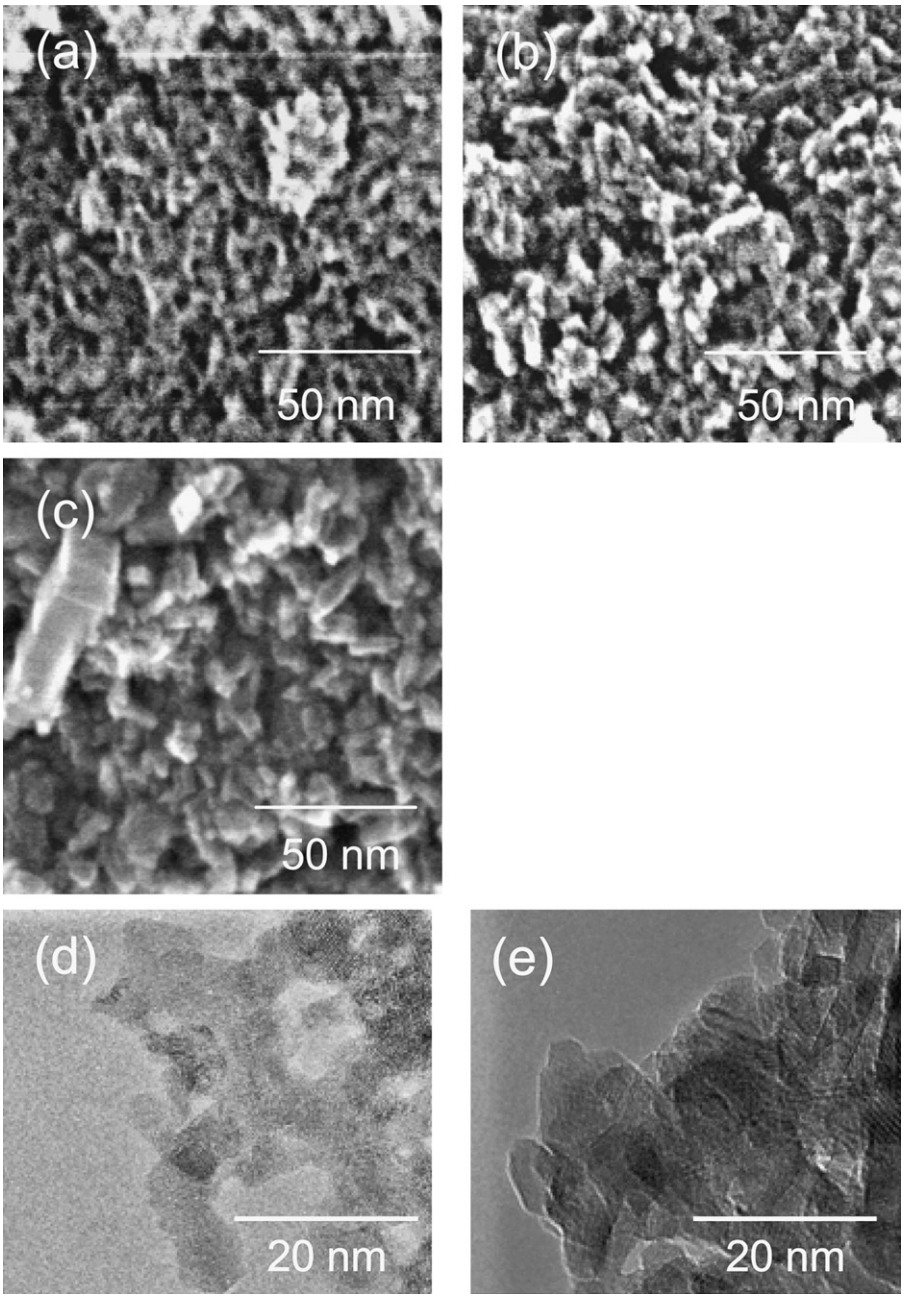

Fig. 3. SEM image of the KIT-6 (a), SEM and TEM images of the samples synthesized (b) and (d) with and (c) and (e) without KIT-6.

3. Results and discussion

Fig. 1 shows the X-ray diffraction patterns of the sample prepared (a) with and (b) without KIT-6. All of the diffraction peaks are assigned to the rutile-type RuO_2 (JCPDS No. 40-1290). Sharp and intense diffraction peaks indicate a high crystallinity. Amorphous RuO_2 is known to have a higher capacitance than the crystalline one [11]. However, we found that the amorphous RuO_2, prepared by lowering the calcining temperature to 423 K, did not retain its porosity during the silica removal process in alkaline solution. We thus examined the influence of the mesoporous structure on capacitive behavior with crystalline RuO_2 as a model substance.

Fig. 2 represents the nitrogen adsorption and desorption isotherms of the samples prepared (a) with and (b) without KIT-6, as well as the pore size distributions calculated from the desorption branch of the isotherm based on the Barret–Joyner–Halenda method. According to the IUPAC classification, the isotherm obtained from sample (a) belongs to the type IV with a hysteresis loop specific to the mesoporous structures [32]. The pore size distribution is narrow and centered at 6.5 nm. On the other hand, the isotherm obtained from sample (b) is classified as the type II, testifying to the absence of mesopores [32]. A tiny peak in the pore size distribution for sample (b) is considered negligible compared to sample (a). The Brunauer–Emmett–Teller (BET) surface areas of samples (a) and (b) are 140 and 39 $m^2\,g^{-1}$, respectively (Table 1). These results indicate that a high surface area RuO_2 material with 6.5 nm mesopores was synthesized using KIT-6. Hereafter, we refer to samples (a) and (b) as the high surface area (HSA) and low surface area (LSA) samples, respectively.

Fig. 3(a)–(c) shows SEM images of KIT-6, HSA and LSA samples, respectively. TEM images of the HSA and LSA samples are also

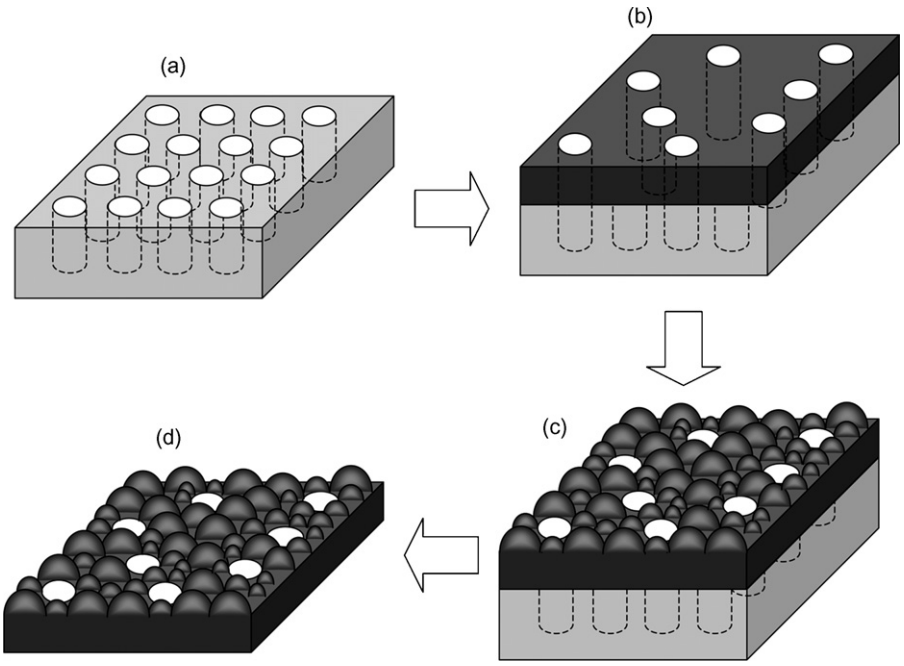

Fig. 4. Schematic illustration of the preparation process. (a) KIT-6 template. (b) The surface of KIT-6 is covered with Ru species leaving some pores reflecting the structure of KIT-6 substrate. (c) The growth of RuO_2 particles on the surface of KIT-6. (d) KIT-6 template is removed.

shown in Fig. 3(d) and (e). The SEM image of the KIT-6 (Fig. 3(a)) proves the presence of dark spots on the particles which we consider as the 8 nm mesopores [30,31]. Similar SEM images of KIT-6 have been reported by Tüysüz et al. [33]. SEM observation of the HSA (Fig. 3(b)) shows that, between particles of which the diameter is 10–20 nm, dark spots resembling those observed for KIT-6 can be seen, though the number density of spots is smaller than the KIT-6. For LSA sample (Fig. 3(c)), on the other hand, the particle diameter is 20–30 nm and no such spot is observed. The TEM observation reveals that the mesoporous structure is present in the HSA (Fig. 3(d)). In contrast to Fig. 3(d), we can only see the aggregation of particles in Fig. 3(e), indicating that LSA is devoid of mesopores. This microscopic observation is consistent with the following considerations based on the surface area. As shown in Table 1, the total BET surface area can be divided into two components: One is the surface area to which the structure of 1–2 nm contributes and the other is the one to which the structure larger than 2 nm contributes. For convenience of the discussion below, we name the former as "microstructure" and the latter as "mesostructure". Let us assume (i) the RuO_2 material has the density of 7.0 g cm^{-3}, (ii) all particles are spherical and (iii) only the "mesostructure" can be observed by SEM (or in other words the "microstructure" is reflected in the surface roughness of the particle). The "mesostructure" surface area of LSA (30 m^2 g^{-1}) is translated into the sphere diameter of 28 nm which is close to what is observed in the SEM image (Fig. 3(c)). For the HSA sample, 6.5 ± 1.5 nm mesopores contribute 30 m^2 g^{-1} to the "mesostructure" surface area of 100 m^2 g^{-1}. The remaining 70 m^2 g^{-1} corresponds to the sphere diameter of 12 nm which is consistent with what is observed in the SEM image of HSA (Fig. 3(b)). In Fig. 4, we speculate the formation process and the morphology of the HSA sample. Fig. 4(a) illustrates a small fraction of a particle surface of KIT-6 of which the diameter is around 1 μm in the present study. During the evaporation of ethanol, the surface of KIT-6 is covered with Ru species leaving some pores reflecting the structure of KIT-6 substrate (b). The thickness of Ru species is ca. 10–20 nm which is inferred from the following quantitative relation: the masses of KIT-6 and the final RuO_2 product are 1.0 g and ∼0.12 g, respectively. The density of KIT-6 is 2.3 g cm^{-3}. Calcination in air at 573 K leads to the growth of the RuO_2 particles on the surface of KIT-6 (c). After removing KIT-6 with alkaline treatment, mesoporous RuO_2 is obtained (d).

As shown in Fig. 5, both the HSA and LSA RuO_2 electrodes retain the rectangular shape of the CV curves in the four electrolytes with the increasing scan rate from 1 to 100 mV s^{-1}, indicating an ideal

Table 2
Specific surface area, specific capacitance in F g^{-1} and capacitance retention of the HSA and LSA RuO_2 electrodes. The values in parentheses are the capacitance per BET surface area in μF cm^{-2}. Error in the specific capacitance indicates twice the standard deviation of the mean (±2σ) based on the results obtained from the samples of three independently prepared batches.

Electrolyte	Surface area (m^2 g^{-1})	Specific capacitance					Capacitance retention (%)
		1 mV s^{-1}	10 mV s^{-1}	20 mV s^{-1}	50 mV s^{-1}	100 mV s^{-1}	C_{100} mV s^{-1}/C_1 mV s^{-1}
HSA RuO_2							
0.5 M H_2SO_4		202 ± 2 (144)	168 ± 1 (120)	161 ± 1 (115)	150 ± 2 (107)	142 ± 3 (101)	70.2 ± 1.0
0.5 M Li_2SO_4	140	81 ± 4 (58)	66 ± 4 (47)	60 ± 4 (43)	56 ± 3 (40)	52 ± 3 (37)	63.5 ± 1.8
0.5 M Na_2SO_4		80 ± 3 (57)	63 ± 3 (45)	58 ± 2 (41)	52 ± 2 (37)	48 ± 2 (34)	59.7 ± 0.7
0.5 M K_2SO_4		81 ± 1 (58)	64 ± 2 (46)	59 ± 1 (42)	52 ± 1 (37)	48 ± 1 (34)	59.5 ± 0.9
LSA RuO_2							
0.5 M H_2SO_4		146 ± 25 (365)	97 ± 25 (243)	89 ± 25 (223)	81 ± 25 (203)	75 ± 25 (188)	61.8 ± 5.3
0.5 M Li_2SO_4	39	50 ± 6 (125)	37 ± 4 (93)	33 ± 4 (83)	30 ± 3 (75)	27 ± 3 (68)	54.3 ± 0.2
0.5 M Na_2SO_4		48 ± 8 (120)	34 ± 5 (85)	31 ± 4 (78)	28 ± 4 (70)	25 ± 4 (63)	52.5 ± 2.8
0.5 M K_2SO_4		47 ± 10 (118)	33 ± 7 (83)	29 ± 6 (73)	25 ± 4 (63)	23 ± 4 (58)	48.0 ± 2.1

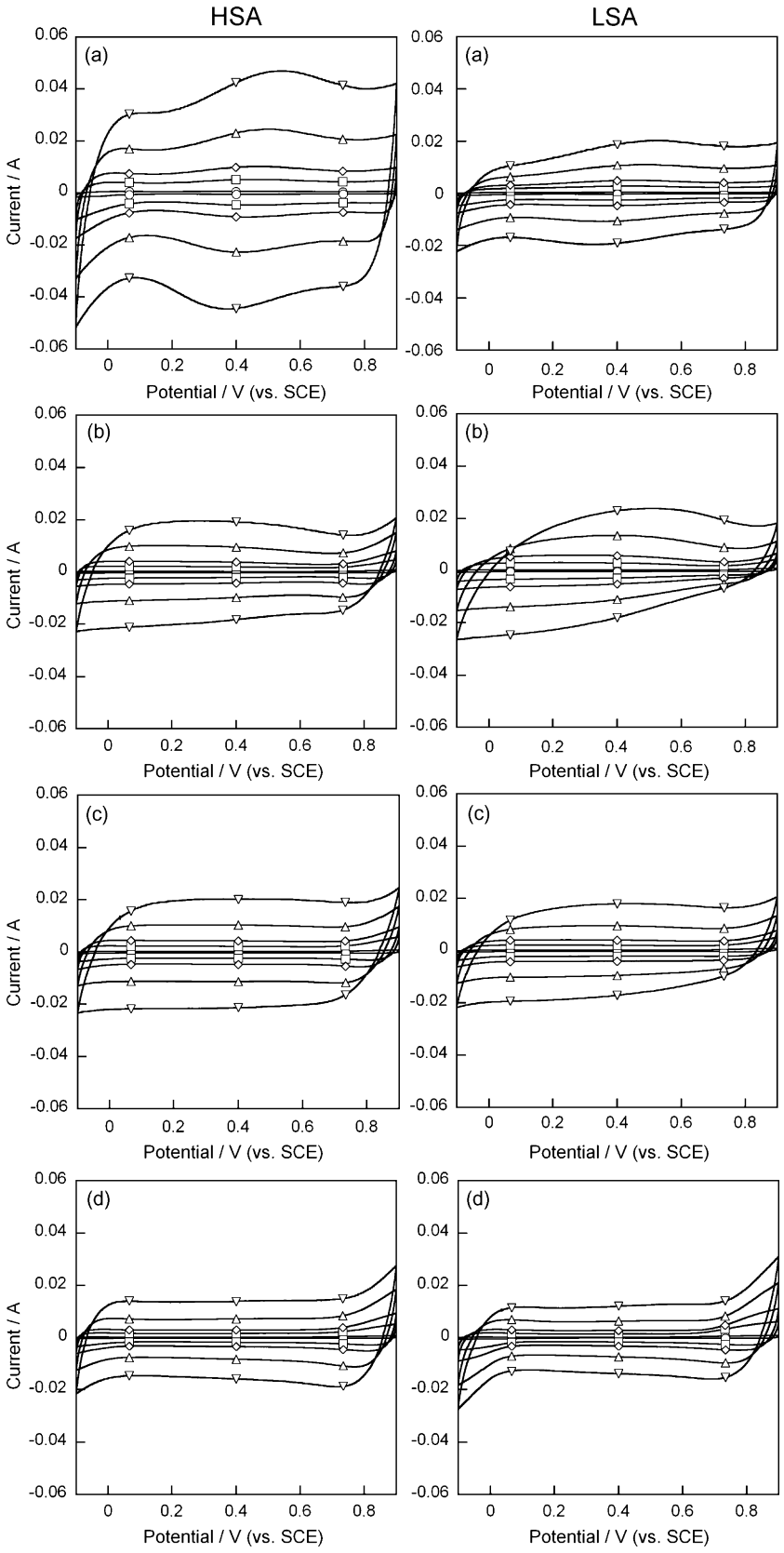

Fig. 5. Cyclic voltammograms of the HSA and LSA RuO_2 electrodes at various scan rates [○ 1, □ 10, ◊ 20, Δ 50, ▽ 100 mV s^{-1}] and in various electrolytes [(a) H_2SO_4 (aq), (b) Li_2SO_4 (aq), (c) Na_2SO_4 (aq), (d) K_2SO_4 (aq)].

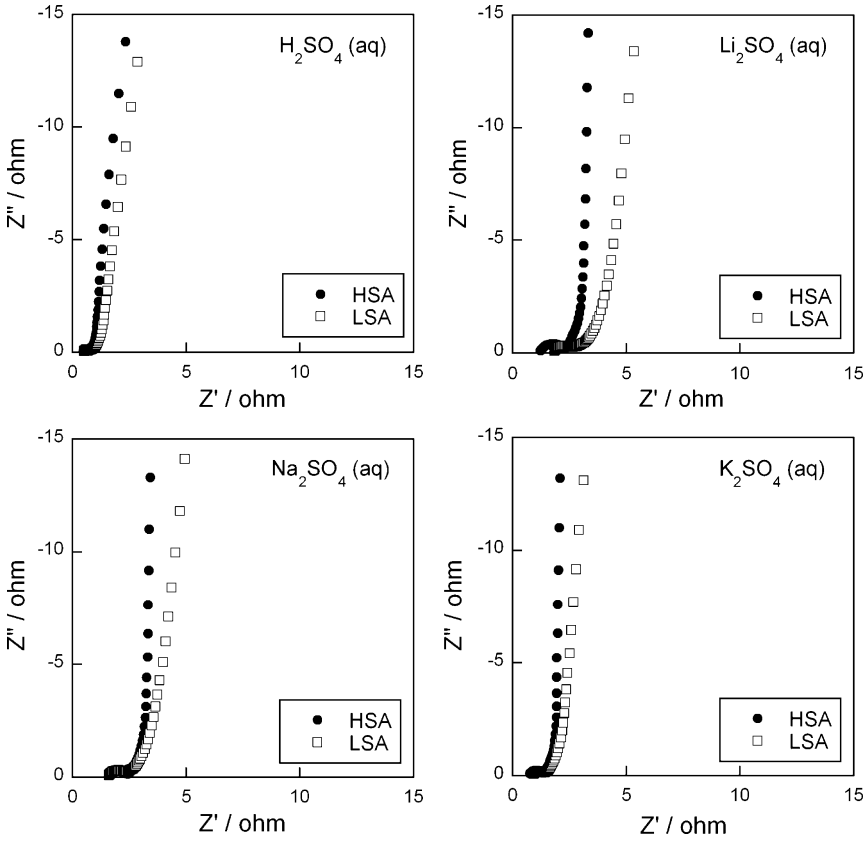

Fig. 6. Electrochemical impedance spectra of the HSA and LSA RuO_2 electrodes.

capacitive behavior. No difference in the CV was observed between the Li_2SO_4(aq) and $LiClO_4$(aq) electrolytes, indicating that the influence of the anion on the electrochemical properties is insignificant. Table 2 summarizes the specific capacitance C in $F\,g^{-1}$ in the different electrolytes and scan rates calculated on the basis of the following equation

$$C = \frac{1}{m\nu(E_b - E_a)} \int_{E_a}^{E_b} I(E)\mathrm{d}E$$

where m is the mass of the active material in the electrode, ν is the scan rate, E_a and E_b are the integration limits of the voltammetric curve and $I(E)$ is the voltammetric charging current [34]. The values in parentheses in Table 2 are the capacitance per BET surface area in $\mu F\,cm^{-2}$.

For the H_2SO_4 electrolyte, both the HSA and LSA electrodes, composed of crystalline RuO_2, have much lower capacitances than the amorphous RuO_2 whose capacitance is $700\,F\,g^{-1}$ or 700–1750 $\mu F\,cm^{-2}$ [11]. We confirmed this high capacitance by measuring the CV of the amorphous RuO_2 prepared in-house which had the capacitance of $670\,F\,g^{-1}$. Barbieri et al. suggested that the amorphous structure and high water content of RuO_2 play an important role in the proton hopping mechanism by which the electrochemical properties of RuO_2 are explained [35]. What causes the difference in capacitive behavior between sulfuric acid and alkali metal sulfates must be complex. However, we can say that it is not due to the difference in pH, because merely an ohmic resistance with a negligible capacitance in the CV was observed when 0.5×10^{-4} mol dm^{-3} H_2SO_4(aq) was used as the electrolyte.

In terms of the capacitance per mass of RuO_2 ($F\,g^{-1}$) the HSA electrode surpasses the LSA electrode, whereas the capacitance of the LSA electrode is twice as high as that of the HSA if compared in terms of per BET surface area ($\mu F\,cm^{-2}$). Zheng and Huang report the capacitance of a crystalline RuO_2 per surface area as 340–480 $\mu F\,cm^{-2}$ [36], whereas a crystalline and mesoporous RuO_2 prepared by Sugimoto et al. has the corresponding value of 200 $\mu F\,cm^{-2}$ [37]. The present result for LSA, 365 $\mu F\,cm^{-2}$, is close to the former reference but significantly larger than the latter. This difference in capacitance per BET surface area seems to be caused by the difference in calcination temperature of the Ru precursor. Differential thermal analysis of Ru precursor shows an exothermic relaxation of crystallization at around 623 K which is just between the calcination temperature of the present study (573 K) and that of Ref. [37] (673 K). Although it is not detectable by XRD, a small

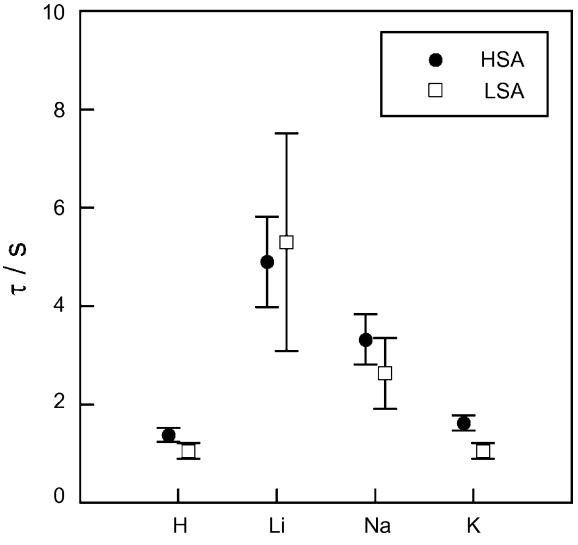

Fig. 7. Response time τ ($=R_0C_0$) of the HSA and LSA RuO_2 electrodes.

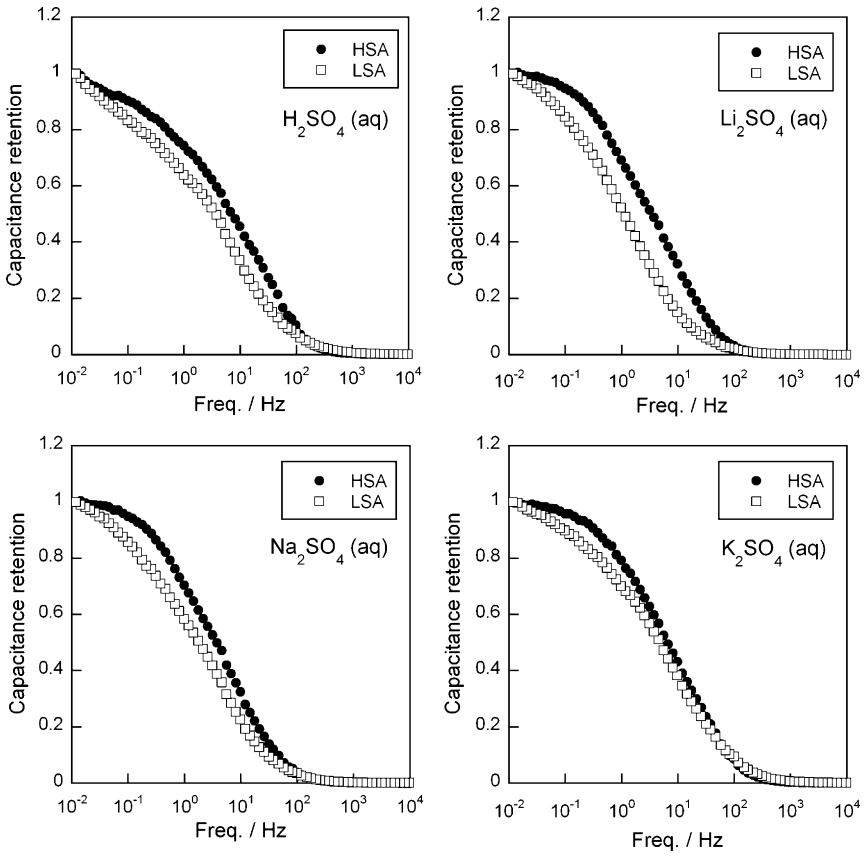

Fig. 8. Frequency dependence of the capacitance retention $C_{x\,Hz}/C_{0.01\,Hz}$ of the HSA and LSA RuO_2 electrodes.

amount of amorphous may remain in the present RuO_2, leading to the higher capacitance of the LSA sample per surface area than that of Ref. [37]. In effect, we found that increasing the calcination temperature of the LSA sample to 673 K led to a drastic decrease in the surface area to 13 $m^2\,g^{-1}$ which is far smaller than the mesoporous crystalline RuO_2 in Ref. [37]. Particle growth associated with crystallization seems responsible for the decrease in the surface area.

Table 2 suggests that increasing the surface area by introducing a mesoporous structure is an effective way to increase the specific capacitance. However, not all the surface in the HSA electrode provides accessible sites for ions to generate the capacitance for which the explanation is yet to be found. Another feature distinguishing the HSA and LSA electrodes is the capacitance retention (C_{100} mV s^{-1}/C_1 mV s^{-1}). The capacitance retention of the HSA electrode exceeds that of the LSA by about 10 points whatever electrolyte is used.

Fig. 6 shows the complex impedance plot (Nyquist plot). In all the electrolytes, both electrodes show an increase in the impedance on the imaginary part (Z'') with the decreasing frequency, which indicates the typical capacitive behavior. If we simulate the impedance by the simplest equivalent circuit in which a resistance R_0 and a capacitance C_0 are connected in series, the response time τ ($=R_0C_0$) of the capacitor is given by the inverse of the frequency at which $\phi = -45$. On the time scale longer than τ, the capacitive behavior prevails over the resistive one [38–40]. As shown in Fig. 7, the order of the response time apparently reflects the reverse order of the mobility and conductivity of the cations in water, i.e. $H^+ > K^+ > Na^+ > Li^+$ [41]. It is interesting that the response time of the HSA electrode coincides with that of the LSA electrode within the experimental error.

Fig. 8 represents the frequency dependence of the capacitance retention [$C_{x\,Hz}/C_{0.01\,Hz}$ ($x = 10000 - 0.01$)] in all the electrolytes. The capacitance was calculated by the relation $C = (2\pi f|Z''|)^{-1}$ where Z'' is the imaginary part of the impedance, f is the frequency, and C is the capacitance [42]. The HSA RuO_2 electrode has a higher capacitance retention than the LSA RuO_2 over the entire frequency range. This observation is consistent with the capacitance retention determined by the CV. For the carbon double layer capacitor [43] and for the conducting polymer pseudocapacitor [44], similar phenomena have been observed that the mesoporous structure results in the higher capacitance retention. For the MnO_2 pseudocapacitor, Luo and xia observed that the ordered mesopores showed a higher capacitance retention than the disordered mesopores [45]. It seems that a common feature of the double layer capacitors and pseudocapacitors is that the mesoporous structure of an electrode produces a high capacitance retention, though the cause of this phenomenon is not yet clear.

For the carbon double layer electrode, micropores with the mean diameter of less than 1 nm lead to a significant increase in the per surface area capacitance and in the response time together with a decrease in the capacitance retention for which distortion in the solvation shell is said to be responsible [46–48]. The mesopore diameter of our RuO_2 electrodes, 6.5 nm, is large enough for solvated cations to enter the pores without any distortion [49], which is presumably reflected in the invariance of the response time between the HSA and LSA electrodes. We can anticipate a maximum in the capacitance retention with respect to the pore size somewhere between the mesopores and micropores. We are now carrying out a further study to understand the relationship among the pore size, carrier size, surface area, capacitance, response time, etc.

4. Conclusions

RuO_2 electrodes with mesoporous structure were prepared using KIT-6 as the template. The mesoporous structure of the RuO_2 electrode results in a high specific surface area which leads to a higher capacitance per mass of RuO_2 than the electrode without mesopores, though the capacitance per BET surface area of the mesoporous electrode is less than that of the one without mesopores. Another benefit of the mesoporous structure is the higher capacitance retention; namely, the mesoporous electrode better maintains its capacitance than the one without mesopores at a higher charging rate. The mesoporous structure of the electrode does not significantly increase the response time of the capacitor when using the aqueous solution of sulfuric acid and alkali metal sulfates.

Acknowledgement

The authors are grateful to the members of the Research Institute for Ubiquitous Energy Devises, especially to Drs. Q. Xu, Z. Siroma, S. Yamazaki and H. Senoh for their helpful suggestions. The authors also thank Mses. E. Takahama and R. Nakamura for their technical assistance.

References

[1] B.E. Conway, Electrochemical Supercapacitors, Kluwer Academic/Plenum Publishers, New York, 1999.
[2] A. Nishino, J. Power Sources 60 (1996) 137.
[3] R. Kötz, M. Carlen, Electrochim. Acta 45 (2000) 2483.
[4] A. Bruke, J. Power Sources 91 (2000) 37.
[5] C. Lin, J.A. Ritter, B.N. Popov, J. Electrochem. Soc. 146 (1999) 3639.
[6] E. Franckowiak, F. Béguin, Carbon 39 (2001) 937.
[7] H. Tamai, M. Kouzu, M. Morita, H. Yasuda, Electrochem. Solid-State Lett. 6 (2003) A214.
[8] J.P. Ferraris, M.M. Eissa, I.D. Brotherston, D.C. Loveday, Chem. Mater. 10 (1998) 3528.
[9] K. Naoi, S. Suematsu, A. Manago, J. Electrochem. Soc. 147 (2000) 420.
[10] F. Fusalba, P. Gouérec, D. Villers, D. Bélanger, J. Electrochem. Soc. 148 (2001) A1.
[11] J.P. Zheng, T.R. Jow, J. Electrochem. Soc. 142 (1995) L6.
[12] V. Srinivasan, J.W. Weidner, J. Electrochem. Soc. 144 (1997) L210.
[13] N. Miura, S. Oonishi, K.R. Prasad, Electrochem. Solid-State Lett. 7 (2004) A247.
[14] V. Subramanian, H. Zhu, R. Vajtai, P.M. Ajayan, B. Wei, J. Phys. Chem. B 109 (2005) 20207.
[15] B.E. Conway, J. Electrochem. Soc. 138 (1991) 1539.
[16] C. Lin, J.A. Ritter, B.N. Popov, J. Electrochem. Soc. 146 (1999) 3155.
[17] C.Z. Deng, R.A.J. Pynenburg, K.C. Tsai, J. Electrochem. Soc. 145 (1998) L61.
[18] J.W. Long, K.E. Swider-Lyons, R.M. Stroud, D.R. Rolison, Electrochem. Solid-State Lett. 3 (2000) 453.
[19] K.R. Prasad, K. Koga, N. Miura, Chem. Mater. 16 (2004) 1845.
[20] C.-C. Hu, K.-H. Chang, M.-C. Lin, Y.-T. Wu, Nano Lett. 6 (2006) 2690.
[21] R.N. Reddy, R.G. Reddy, J. Power Sources 156 (2006) 700.
[22] X.-H. Yang, Y.-G. Wang, H.-M. Xiong, Y.-Y. Xia, Electrochim. Acta 53 (2007) 752.
[23] M.-S. Wu, Y.-A. Huang, C.-H. Yang, J.J. Jow, Int. J. Hydrogen Energy 32 (2007) 4153.
[24] G.M. Suppes, B.A. Deore, M.S. Freund, Langmuir 24 (2008) 1064.
[25] K.-C. Liu, M.A. Anderson, J. Electrochem. Soc. 143 (1996) 124.
[26] F. Fusalba, N. El Mehdi, L. Breau, D. Bélanger, Chem. Mater. 11 (1999) 2743.
[27] A. Celzard, F. Collas, J.F. Marêché, G. Furdin, I. Rey, J. Power Sources 108 (2002) 153.
[28] S. Álvarez, M.C. Blanco-López, A.J. Miranda-Ordieres, A.B. Fuertes, T.A. Centeno, Carbon 43 (2005) 855.
[29] D.-W. Wang, F. Li, H.-T. Fang, M. Liu, G.-Q. Lu, H.-M. Cheng, J. Phys. Chem. B 110 (2006) 8570.
[30] F. Kleitz, S.H. Choi, R. Ryoo, Chem. Commun. 17 (2003) 2136.
[31] T.-W. Kim, F. Kleitz, B. Paul, R. Ryoo, J. Am. Chem. Soc. 127 (2005) 7601.
[32] S.J. Gregg, K.S.W. Sing, Adsorption, Surface Area and Porosity, second ed., Academic Press, London, 1982.
[33] H. Tüysüz, C.W. Lehmann, H. Bongard, B. Tesche, R. Schmidt, F. Schüth, J. Am. Chem. Soc. 130 (2008) 11510.
[34] V. Panic, T. Vidakovic, A. Gojkovic, A. Dekanski, S. Milonjic, B. Nikolic, Electrochim. Acta 48 (2003) 3805.
[35] O. Barbieri, M. Hahn, A. Foelske, R. Kötz, J. Electrochem. Soc. 153 (2006) A2049.
[36] J.P. Zheng, C.K. Huang, J. New Mater. Electrochem. Syst. 5 (2002) 41.
[37] W. Sugimoto, T. Kizaki, K. Yokoshima, Y. Murakami, Y. Takasu, Electrochim. Acta 49 (2004) 313.
[38] P.L. Taberna, P. Simon, J.F. Fauvarque, J. Electrochem. Soc. 150 (2003) A292.
[39] D. Susanti, D.-S. Tsai, Y.-S. Huang, A. Korotcov, W.-H. Chung, J. Phys. Chem. C 111 (2007) 9530.
[40] W. Sugimoto, H. Iwata, K. Yokoshima, Y. Murakami, Y. Takasu, J. Phys. Chem. B 109 (2005) 7330.
[41] S. Wen, J.-W. Lee, I.-H. Yeo, J. Park, S.-I. Mho, Electrochim. Acta 50 (2004) 849.
[42] H.-Q. Li, J.-Y. Luo, X.-F. Zhou, C.-Z. Yu, Y.-Y. Xia, J. Electrochem. Soc. 154 (2007) A731.
[43] A. Izadi-Najafabadi, D.T.H. Tan, J.D. Madden, Synth. Met. 152 (2005) 129.
[44] J. Wang, Y. Xu, X. Chen, X. Du, J. Power Sources 163 (2007) 1120.
[45] J.-Y. Luo, Y.-Y. Xia, J. Electrochem. Soc. 154 (2007) A987.
[46] C. Vix-Guterl, E. Frackowiak, K. Jurewicz, M. Friebe, J. Parmentier, F. Bégium, Carbon 43 (2005) 1293.
[47] J. Chmiola, G. Yushin, R. Dash, Y. Gogotsi, J. Power Sources 158 (2006) 765.
[48] J. Chmiola, G. Yushin, Y. Gogotsi, C. Portet, P. Simon, P.L. Taberna, Science 313 (2006) 1760.
[49] Y. Marcus, Ion Properties, Marcel Dekker Inc., New York, 1997.